UNIVERSITY OF CALIFORNIA

SANTA CRUZ

Evolution of Human Brain Development

A thesis submitted in partial satisfaction
of the requirements for the degree of

MASTER OF ARTS
in
MOLECULAR, CELL AND DEVELOPMENTAL BIOLOGY

by

Gary Mantalas

December 2022

The thesis of Gary Mantalas is approved by:

Dr. David HAUSSLER

Dr. Sofie SALAMA

Dr. Mircea TEODORESCU

Dr. Bin CHEN

Peter BIEHL
Vice Provost and Dean of Graduate Studies

Contents

Figures

Abstract

Evolution of Human Brain Development

Gary Mantalas

Understanding what makes us human is a major goal in biology. Humanity is marked by our ability to learn from the lessons of our ancestors; a capacity that was bestowed on us through the evolution of our cerebral cortex. An expansion of our forebrain has undergone a 4-fold expansion over the last 3.5 million years. Neurodevelopmental evidence points to gene duplications in the 1q21.1 region as contributing to human specific differences in cranial volume. This thesis aims to further the goal of understanding the evolution of human brain development through two fronts. First, combining genetically engineered knockouts of regions of 1q21.1 with stem cell derived models of the developing brain and single cell transcriptome sequencing we provide evidence of the role of NOTCH2NL in stem cell maintenance and lineage choice. NOTCH2NL knockout cell lines demonstrate decreases in the number of late derived neurons as well as a population of cells in the osteoblast lineage expressing PDGFRB and

lacking PDGFRL expression. This suggests that by accelerating late neurogenesis and increasing skull bone production, NOTCH2NL is the causative mutation in 1q21.1 neurodevelopmental pathologies. Second, we engineer physical automation tools around stem cell derived models of the developing brain to better mimic physiology in these models. We show that our model augments the expression of glycolysis pathway genes towards expression levels found in the human body, potentially fixing the biggest observed differences in traditional cerebral organoid models from their physiological counterparts.

Acknowledgements

First I would like to thank my advisors, Sofie Salama and David Haussler for guidance and mentorship throughout my graduate studies. I admire David's progressive vision in how to optimally advance our understanding of human evolution and Sofie's ability to lead a complex interdisciplinary research group while maintaining deep understanding of each individual project within the group. I am forever grateful for the experiences that I gained under their guidance.

Prior to coming to UCSC I have received considerable mentorship from many excellent advisors. Stephen Quake at Stanford University helped me to understand how much can be accomplished by a small group of very smart people and also helped me to learn cutting edge technologies in the biotech field. Daniel Morse at UCSB taught me the importance of experimental patience and how to look for clues to solving complex problems by learning lessons from biology and evolution.

At UCSC I am grateful for the mentorship I received from many individuals. Mircea Teodorescu brought his knowledge

of mechanical engineering that is unmatched at UCSC and an enthusiasm level that keeps everyone excited to contribute to the cause. Bin Chen and Alex Pollen offered key insights into data that pointed me in the direction that the NOTCH2NL story took. Kristof Tigyi, Bari Nazario, and Andrew Field taught me techniques that were invaluable to my studies.

I am grateful for the support that I received from my family. During my time at UCSC I needed a lot of support both within my studies and in my personal life. I married my longtime girlfriend Eunice Camille Fangon, and had my two children Oliver Clark and Alina Rose during my time in Santa Cruz. I also suffered the loss of both of my parents during this same time. Being able to maintain a focus on my studies during this tumultuous time required the stability that I found from my wife Eunice and her family as well as from my sister Amber. Without their help I could not have done this work.

Introduction

Where Did Big Brains Come From?

The human brain is an enigma. 3 Million years ago something evolved in the way that our brains developed that set us off on a journey leading to the higher orders of cognitive thought that gave rise to civilization, culture, and technology found around the world today. Scientists have been seeking to find the genetic cause that occurred in our lineage since the theory of evolution was proposed. While several interesting candidates have been proposed, the identification of the specific element has proven to be difficult[1]. One major hindrance to researchers has been the lack of an adequate platform for testing new hypotheses[2]. Here we discuss interesting candidate genes, NOTCH2NLA and NOTCH2NLB as well

as improvements to the cerebral organoid – a model of the developing human brain.

NOTCH2NL genes arose in our lineage when a duplication and subsequent gene conversion from the N-terminus of a signaling gene called NOTCH2[3]. The functional version of NOTCH2NL found in human genomes is estimated to have arisen approximately 3 million years ago[3]. This timing correlates with archeological evidence of the onset of the fourfold expansion found in our cranial and cerebral cortex volume[3]. NOTCH2NL has a similar gene expression pattern to its ancestral gene, NOTCH2[1]. NOTCH2 is a cell surface receptor involved in conveying proliferative signals from signaling cells to stem cells in the brain called radial glia[4]; this leads to more substrate to generate cranial mass from. It has been shown that NOTCH2NL, a secreted protein, is able to activate NOTCH2 exogenously[3]. By activating NOTCH2, NOTCH2NL

could be one of the genes that paleogenomics researchers have been searching for.

We studied the effect of altering copy number of NOTCH2NL on the developmental program. This was done by engineering deletions of NOTCH2NL loci in the human embryonic stem cell line H9 and growing cerebral organoids to measure the changes to cell types throughout the first 4 months of brain development. We found that not only was there a twofold decrease to the upper layer neuronal population in the deletion cell lines compared to wild type. We also serendipitously found fivefold increases in the counts of proliferative ectomesenchyme cell populations that express proteoglycan genes, cells involved in skull development. This suggests that NOTCH2NL ties together the control of cranial and brain volumes by increasing the populations of these precursor cells in parallel.

To study neurodevelopment it is important to have a high fidelity model. The aggregation and

differentiation of pluripotent stem cells into three dimensional organoids offers a platform to study human development and pathologies *in-vitro[2]*. However, recent work with cerebral organoids has identified expression of cell stress genes as well as an impaired subtype specification in the most common protocols of differentiation that is reversible when transplanted *in-vivo[5,6]*. This brings into question the translation of *in-vitro* findings, especially for sensitive measurements of derived cells such as neurons. To improve the accuracy of our model we engineered a

system to better mimic physiology termed the Autoculture system. Studying the developing human brain has only recently become within reach. By adding layers of genetic engineering and biological mimicry to current models, this dissertation enriches our understanding of human brain development.

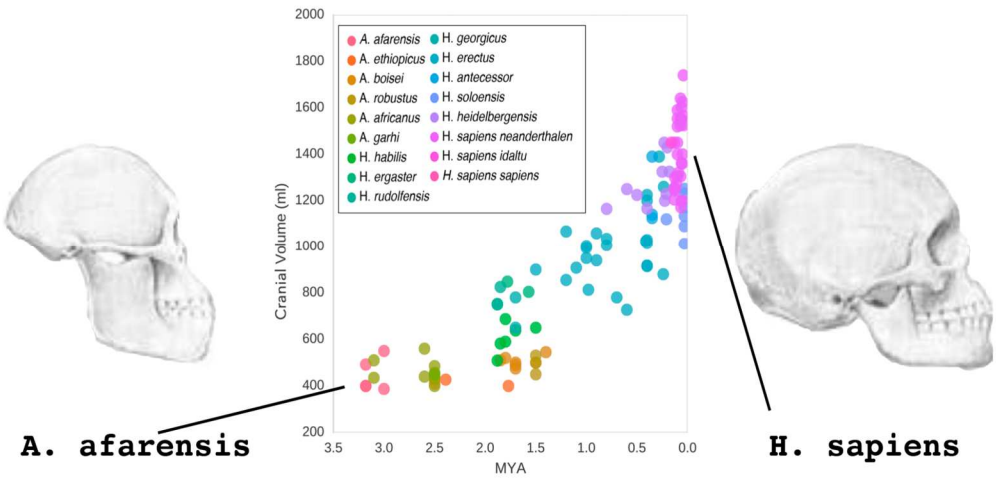

Figure 1: Fourfold expansion of human cranial volumes. Archaic human cranial volumes were calculated from fossil record measurements over the past 3 million years. (Adapted from Fiddes et al. Cell 2018)

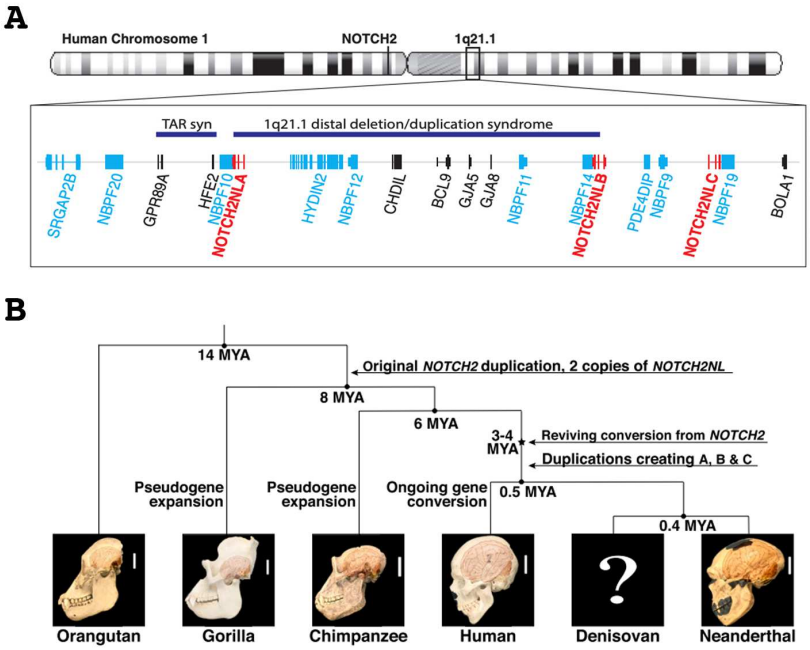

Figure 2: NOTCH2NL evolution occurred in multiple steps. *(A) Chromosomal region 1q21.1 contains duplicated genes (colored) including 3 NOTCH2NL loci. (B) NOTCH2NL evolved from a duplication of the N-terminus of NOTCH2 and subsequent gene conversion correcting the non-functional gene in our ancestors 3-4M years ago. (Adapted from Fiddes et al. Cell 2018)*

Chapter 1

NOTCH2NL

Background

Human Specific Structural Differences

The development of the human brain starts during neural groove formation, a structure on the dorsal side of the developing embryo where ectoderm cells gradually fold, eventually forming a closed tube at about 28 days post conception[9]. Of the many cell types that are derived from the neural ectoderm, an important progenitor cell class called radial glia gives rise to billions of neurons and glial cells

including astrocytes and oligodendrocytes in the fully developed human brain[9]. Radial glia exist on extended fibers that reach from the ventral surface of fluid filled ventricles interior to

the brain to the pial surface on the exterior[9]. In humans, there is an expansion to the number of a class of radial glia derived later in development called outer radial glia (oRG) whose extensions are no longer connected to the ventral surface and whose cell bodies are positioned in the outer subventricular zone[10]. As neurons are formed they migrate outward along the fiber extensions into layered structures with functional significance[9]. The thickness of these functional layers differs in different species and in different regions of the brain[11]. While each of the layers of the cortex have been expanded in humans, the upper layers (II/III) have gone through a more marked expansion[12]. While both ventral radial glia (vRG) and oRG give rise to these upper layer neurons, oRG have been shown to be the primary source of upper layer neurons in humans[10].

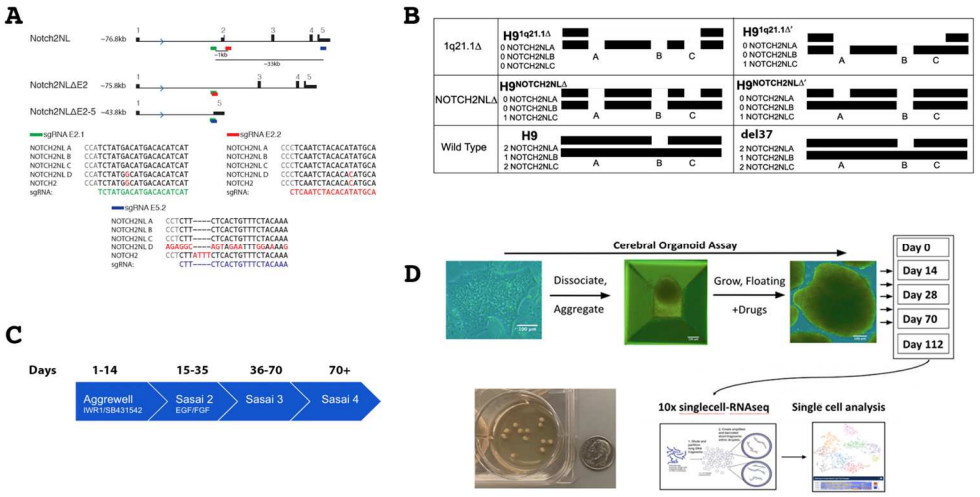

Figure 3: Cell type abundance measurements in NOTCH2NL deletion lines. *(A) Design of CRISPR guide RNAs. (B) Cartoon diagram of sample genotypes, two black bars represent homologous chromosome 1 pairs, white portions are deletions as observed in Chromium 10x synthetic long read sequencing. (C) Feeding schedule (D) Cerebral organoid assay flow chart.*

Results

Sample Generation and Sequencing

Organoids of six genotypes were grown: wild-type H9, two genotypes with localized deletions around NOTCH2NL genes (NOTCH2NL□ and NOTCH2NL□'), two genotypes with heterozygous deletions of the entire region between NOTCH2NLA and NOTCH2NLC including NOTCH2NLB (1q21.1□ and 1q21.1□') and an additional sample that was put through the gene editing process but deletions of NOTCH2NL were not observed (del37). We performed single-cell RNAseq prep at days 0, 14, 28, 35, 70, and 113. Unfortunately the cell dissociations at time points 28 and 35 took too long and ended up not having enough high quality cells for downstream sequencing.

Figure 4: Unbiased clustering of single cell data.

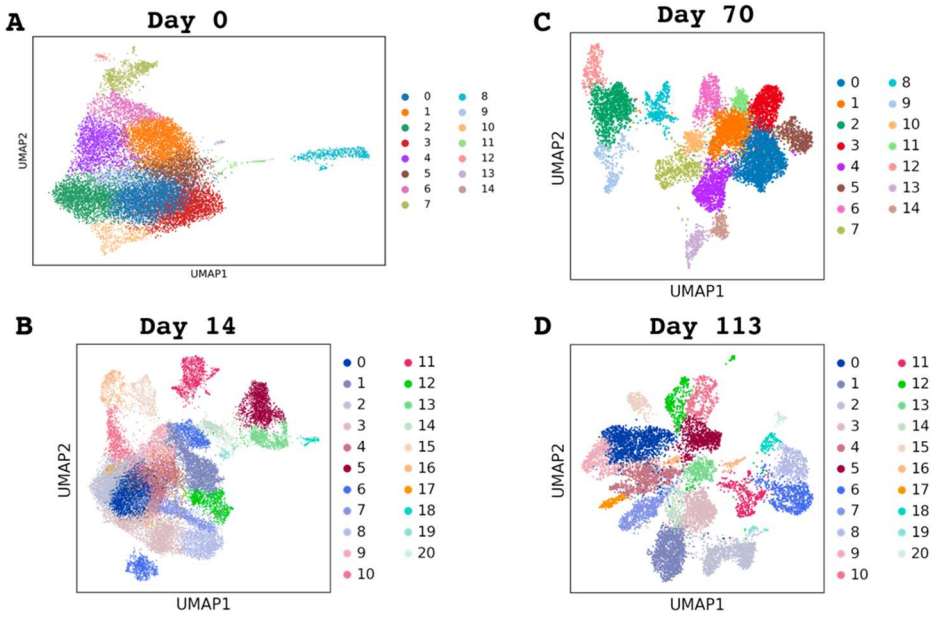

Multidimensional clustering of RNAseq data from (A) hES cells (B) 2 week organoids (C) 10 week organoids and (D) 113 day organoids. Each dot represents a single cell and proximity represents similarity of gene expression matrices. Clusters of cells representing similar cell states are identified and colored.

Samples were clustered using an unbiased approach generating 14 clusters at day 0, 20 clusters at day 14, 14 clusters at day 70, and 20 clusters at

day 113 (Figure 4). At day 14 we identified clusters of neuroepithelium (clusters 0 and 17), radial glia (clusters 1, 6, 9, and 19), Cajal-Retzius neurons (cluster 15 and 16), cranial neural crest cells (clusters 5, and 13), a mitotic cycle (from cluster 3 to 8 to 7), cranial neural crest derived ectoderm (cluster 11), and developing neocortex (cluster 12). Day 70 cells were overwhelmed by mitochondrial and metabolic genes, likely due to this stage representing a dynamic shift in cell identity. Because of the significant noise that this gene expression represented, the clusters of this time point were ambiguous and it was not used for further analysis. At day 113 we identified clusters of neurons (clusters 0, 1, 3, 9, and 14), dividing cells (cluster 10 dividing into 12), two clusters expressing dorsal root ganglia genes such as *SEMA6D* (clusters 2 and 19), one cluster expressing olfactory bulb genes such as *DLX5*, *DLX1*, and *DLX6-AS1* (cluster 15), one cluster expressing cranial muscle genes such as *MYL9*, *TAGLN*, and *TPM2*

(cluster 11) and proteoglycan producing ectomesenchyme cells (clusters 6, 8, and 18). Within the neuronal clusters of day 113, we observed clusters of recently derived neurons (clusters 1, 3 and 14), metabolic neurons (cluster 4), inhibitory neurons (clusters 7 and 17), and deep layer neurons (clusters 0 and 9). Pseudotime analysis of the day 113 sample generated four continuous threads (figure 5). The primary thread contained a spectrum of neurons with a fork leading to clusters of glial cells such as astrocytes and choroid plexus. The second largest thread contained clusters of cranial neural crest derived cells. The remaining two threads represented the olfactory neuron cluster and dorsal root ganglion clusters. 0. At day 14 we observed a significant decrease in the percentage of ectomesenchyme derived cells in the CRISPR modified clusters.

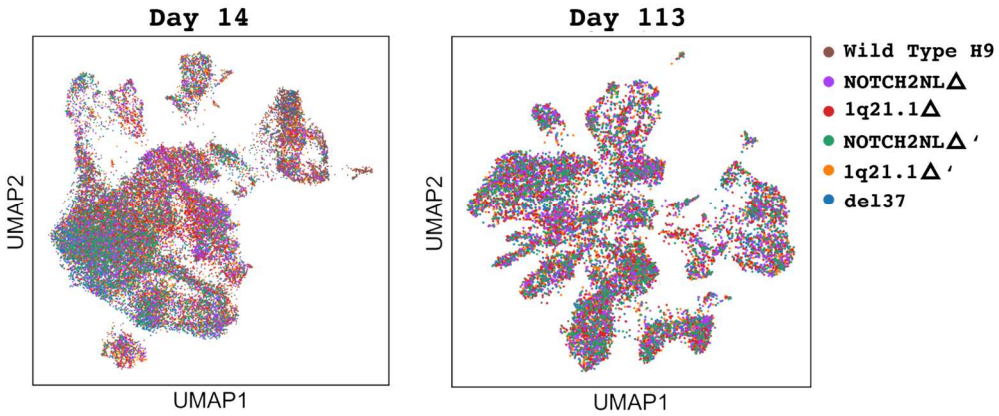

Figure 5: Cluster representation not biased by sample. *Cells colored based on the input genotype*

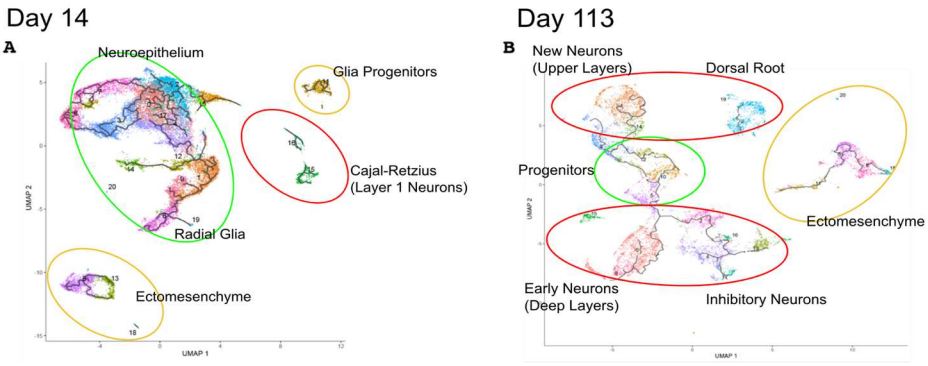

Figure 6: Monocle 3 pseudotime analysis. *Two dimensional representation of cell type continuums. Localization of cell types at 2 weeks (A) more condensed around apical progenitors and week 16 (B) is more distributed with apical progenitors closer to the center. Cell trajectories stem from progenitors (green circles) to either ectodermal lineages (red circles) or ectomesenchymal (yellow circles).*

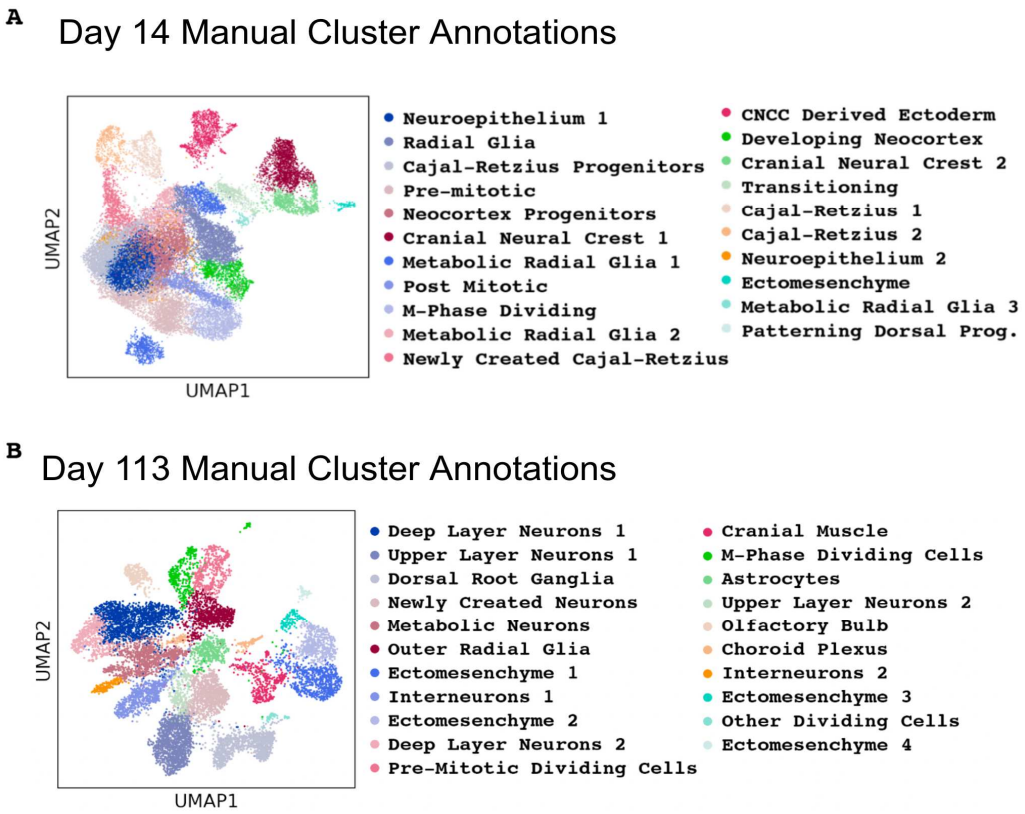

Figure 7: Manual identification of cluster identities. *The same UMAP projections from figure 4 with clusters named based on expression of indicative genes and relationship of cell types in pseudotime analysis.*

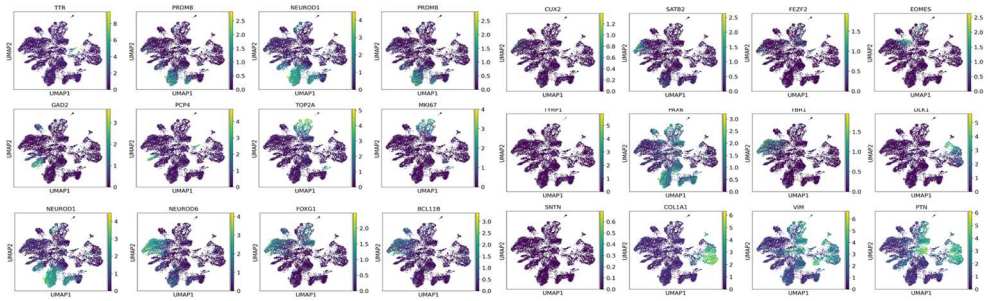

Figure 8: Gene expression of representative genes from day 113 organoid sample. *The same UMAP projections from figures 4, 5 and 7 recolored by gene expression values from some of the genes used to identify cell types in figure 7B.*

Genotypic Differences

Comparing cell type abundances between wild type H9 and CRISPR modified clones of H9 we observed no significant differences at day cell lines. At day 113 we observed significant decreases in the percentage of cells

for clusters 2, 4, 13, 14, 15, and 20 in the CRISPR modified cell lines. Estimating cell abundances on the day 113 data with the CRISPR clone depleted clusters removed (2, 4, 13, 14, 15, and 20) resulted in the remaining clusters having no significant differences between the wild type and CRISPR edited genotypes.

The CRISPR clone line del37, whose 10x Chromium synthetic long read sequencing data did not identify any NOTCH2NL engineered deletions was hypothesized to perform identical to wild type H9. However, our findings disagreed with this hypothesis where at days 14 and 113 the CRISPR clone line del37 more accurately recapitulated

the cell type abundance distribution of the other CRISPR clone lines (NOTCH2NL and 1q21.1 deletion lines).

A

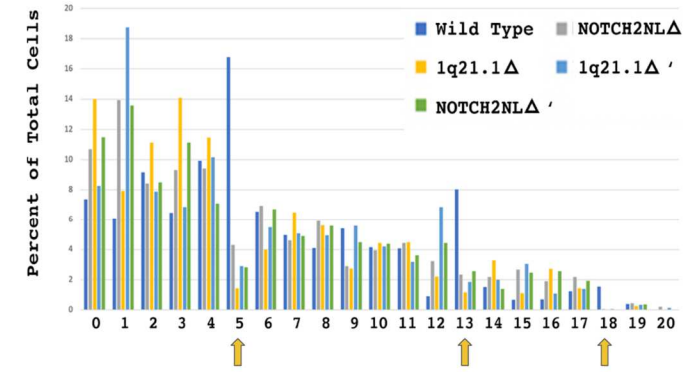

0. Neuroepithelium 1
1. Radial Glia
2. Cajal-Retzius Progenitors
3. Pre-mitotic
4. Neocortex Progenitors
5. Cranial Neural Crest 1
6. Metabolic Radial Glia 1
7. Post Mitotic
8. M-Phase Dividing
9. Metabolic Radial Glia 2
10. Newly Created Cajal-Retzius
11. CNCC Derived Ectoderm
12. Developing Neocortex
13. Cranial Neural Crest 2
14. Transitioning
15. Cajal-Retzius 1
16. Cajal-Retzius 2
17. Neuroepithelium 2
18. Ectomesenchyme
19. Metabolic Radial Glia 3
20. Patterning Dorsal Prog.

B

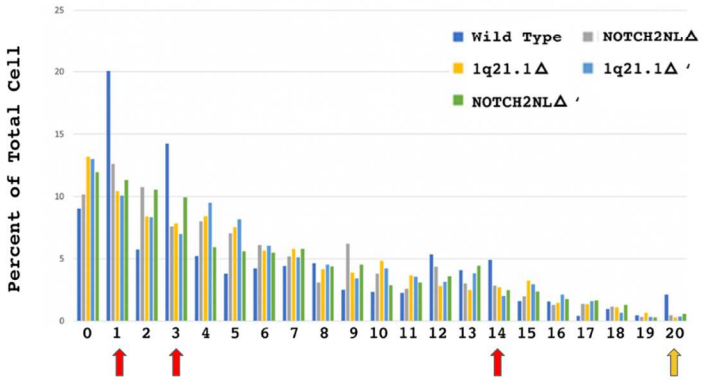

0. Deep Layer Neurons 1
1. Upper Layer Neurons 1
2. Dorsal Root Ganglia
3. Newly Created Neurons
4. Metabolic Neurons
5. Outer Radial Glia
6. Ectomesenchyme 1
7. Interneurons 1
8. Ectomesenchyme 2
9. Deep Layer Neurons 2
10. Pre-Mitotic Dividing Cells
11. Cranial Muscle
12. M-Phase Dividing Cells
13. Astrocytes
14. Upper Layer Neurons 2
15. Olfactory Bulb
16. Choroid Plexus
17. Interneurons 2
18. Ectomesenchyme 3
19. Other Dividing Cells
20. Ectomesenchyme 4

Figure 9: Differences in the representation of cell types by genotype. *The percentage of total cells in each cluster from figures 4 and 7. The most abundantly enriched cell types for wild-type vs mutant were ectomesenchyme (yellow arrows) in both time points and newly created neurons (red arrows).*

Conclusions

Evolution is never simple, humans are no exception. Our cognition increases required not only increases to the complexity of our thought centers but coordinated coevolution of bone geometries. Notch2nl first increases cranial neural crest which makes sense as this leads to the production of osteocyte progenitors and tissue growth would be stunted by physical constraints if this happened later. In the process of removing stem cells from the pool of neuronal

progenitors to create cranial neural crest cells, Notch2nl delays the production of the neocortex.

Neuronal production with NOTCH2NL expression eventually catches up. The longer window of time where radial glia are productive is expanded and shifted later in NOTCH2NL expressing tissues. This results in particularly significant increases to the number of late stage neurons found in upper layers. Later time points, once neuronal production is closer to complete, would better identify “upper layer” neurons from “newly created” neurons and result in a better demarcation of the layered differences between genotypes.

This experimental design was particularly noisy, stochastic differences between experimental models required the implementation of barcoding to increase sample duplication level. This noise makes it difficult to draw conclusions between the different mutant genotypes. This problem is compounded by the difficulty in genotyping 1q21.1

with high resolution. The fact that del37 did not recapitulate the findings of wild type as was predicted in the experimental design is a major caveat to this research. The rescue of NOTCH2NL expression in deletion lines could go a long way in validating the findings here. This could be done by either supplying Notch2nl protein exogenously or engineering rescue lines with functional NOTCH2NL returned to the genome. Histologically interesting time points are dynamic resulting in noisy gene expression. In day 70 cerebral organoids this meant that a majority of the cell populations were unidentifiable. Because the collection of transcripts in these cells are overwhelmingly metabolic, this probably can't be solved informatically. One solution is to select time points for single cell RNAseq analysis that are more stable in cellular identity. As these transitions are probably short lived, looking a week earlier or later may have been sufficient. Sequencing with more temporal resolution and

performing a continuous pseudotime analysis, while tedious, would be extremely insightful in telling the whole story.

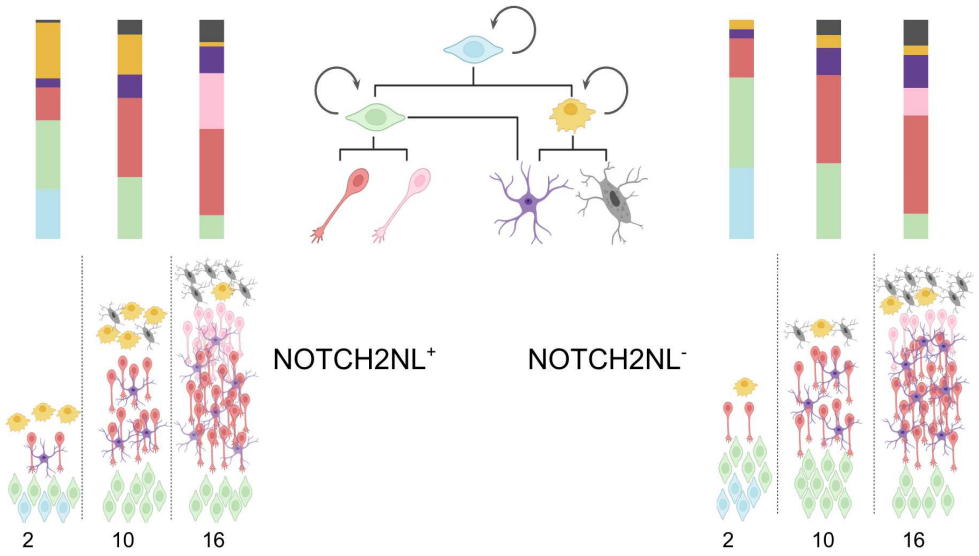

Figure 10: Proposed model of NOTCH2NL developmental control. Differentiation tree (top middle) shows ectomesenchyme and neural progenitor pools stemming from a common cell type. Cell type abundances were assigned to one of each of 7 cell types (common progenitor in blue, neural progenitor in green, ectomesenchyme progenitor in yellow, old neuron in red, young neuron in pink, glial lineage in purple, or proteoglycan producing cell in gray). Bar graphs and visual representations represent abundances from weeks 2, 10 and 16 for wild type (left) and an aggregation of mutant genotype data

(right).

Methods

Cell and Organoid Culture

Human embryonic stem cell lines H9, del37, del42 (NOTCH2NL□), del70 (NOTCH2NL□'), del61 (1q21.1□), and del58 (1q21.1□') were grown on human vitronectin treated tissue culture plates in StemFlex Cell Culture Medium. Feeding was performed every other day and subpassaging was performed approximately every 5 days with a feed occurring the day after passage. Subculture dissociations were performed by incubating in 0.5mM EDTA for approximately 3 minutes, although this time was titrated on a per lot basis for optimal cluster size and density. To generate cerebral organoids, cultures were dissociated to single cells using Accutase Cell Dissociation Reagent and washed in DMEM/F12. Cells were counted using trypan blue, cultures with a viability of over 90% were used for subsequent organoid aggregations. Low adherence treated Aggrewell 800, 24 well plates were loaded with 3M cells per

well in Aggrewell Medium supplemented with ROC inhibitor and spun down at 100xG for 5 minutes. On the following day (day 1), half of the media was replaced with Aggrewell Medium containing 0.1% SB431542 and IWR-1 (Agg). On day 2, organoids were flushed out of the plates and filtered on a 37 um strainer to transfer to a 6 well ultra low adherence plate in 3mL Agg media. Feeds were performed every day until day 6 and every other day until day 14 replacing half of the media with fresh Agg media. Feeds continued every other day using DMEM/F12 glutamax supplemented with N2, and lipid concentrate with fresh 0.1% FGFb and EGF added. From day 35, the media had EGF/FGF replaced with FBS. On day 70 the media additionally contained B12 supplement.

Organoid Dissociation

Organoid sets were placed in a well of two 24 well plates. Organoids were then cut in half using two 24G needles to release the necrotic slurry from

the center and leave the living outer tissue intact. Remaining tissues were washed with DMEM/F12 to remove dead slurry and remaining culturing buffer. After aspirating off DMEM/F12, 400uL of room temperature accutase was added to each well. Samples were incubated in accutase at 37C for 10min. Samples were then broken up by manually pipetting up and down using a p200 pipette and filtered through 2cm flow cytometry filter squares into labeled 15mL conicals to remove clumps. Samples were spun at 300x g for 5min, media was aspirated and samples were resuspended in 100 uL culturing medium (Aggrewell or Sasai media) + ROC inhibitor and kept on ice. Cells were counted using a Biorad automated hemocytometer to normalize for MultiSeq oligonucleotide staining.

MultiSeq Oligonucleotide Staining

This portion of the protocol was carried out in the 4C room, cold temperatures are critical to

maintain barcodes on cells. Cells were labeled using the MultiSeq reagents and protocols obtained from the McGinnis lab at UCSF. Prior to cell collection barcodes were prepared by mixing anchor and barcode in 1:1 molar ratios for each of 28 unique barcodes by combining 1.1uL LMO anchor, 15.4uL DPBS and 5.5uL barcodes into 4 wells (one per replicate) of 7 strip tubes (one per genotype) to the other four wells of each strip tube 1.1uL of LMO co-anchor was mixed with 21uL DPBS. Swinging bucket centrifuge was chilled to 4C. Day 0 samples were collected from extra cells remaining after dissociating and counting for aggregation. Day 14, 35, 42, 70, and 113 samples were collected and counted as described above. If the total number of cells was greater than 500k, samples were diluted to 2.6M cells/mL, otherwise they were brought to 180uL. 180uL of each sample was distributed into 1.5mL conical tubes. To each sample 20uL of a unique barcode:anchor mix was added and then was incubated for 5 minutes on ice. Sample barcodes

were recorded. After 5 minute incubation, a 20uL co-anchor solution was added to each sample and an additional 5min incubation was performed on ice. After the second incubation, 1mL of a 1% BSA solution in DPBS was added. Three washes were performed in 1.2mL 96-well plates by spinning at 300x g for 3min at 4C and aspirating the BSA solution followed by resuspending the cells in 200uL 1% BSA. All 28 samples were combined, filtered and counted for 10x microfluidic reverse transcription reaction.

cDNA synthesis

Single Cell RNAseq library preparation was performed using the 10x protocol with v3 and v3.1 chemistries. Reagents were thawed and stored on ice. 10x Reaction mixture was made as described in table 1. Technical replicates were performed on each of 6, 10x wells by splitting the 28 sample MultiSeq mixtures from above into 6, 25,000 cell aliquots in 40uL DPBS and adding 30uL of the 10x

Table 1: Molecular Biology Recipes	
10x Reaction Mixture (Day 1)	
RT reagent	124.08 uL
Template switch oligo	15.84 uL
Reducing reagent B	13.2 uL
RT Enzyme C	57.42 uL
Dynabeads Cleanup Mix (Day 2)	
Cleanup buffer	1201 uL
Dynabeads MyOne Silane	52.8 uL
Reducing agent B	33 uL
Water	33 uL
Elution Solution I (Day 2)	

EB	980 uL
10% Tween 20	10 uL
Reducing reagent B	10 uL
Barcode Amplification Mix (Day 2)	
2x Kapa HiFi amp mix (no primers)	26.25 uL
Universal i5 primer	2.5 uL
RPI primer (unique per lane)	2.5 uL
3.5 ng DNA	Volume based on qubit
Water	To 50 uL

reaction mixture. 70uL of each sample was added to 6 row 1 wells of 10x chip G. 50% glycerol was loaded into empty lanes. Row 2 was filled with 50uL of gel beads that had been vortexed for 30 seconds and row 3 was filled with 45uL

partitioning oil. Chip was covered with gasket and loaded in chip loader onto the 10x instrument. Protocol was run. After run completed volumes and emulsion integrity were visually inspected. 100uL of each sample was slowly transferred (20 second aspiration) to a 96 well plate and sealed. Reverse transcription was carried out by incubating on a thermal cycler for 45 minutes at 53C followed by 5 minutes at 85C. Samples were stored at 10C until second strand synthesis was performed.

Primary Amplification Product Cleanup

For each of six 10x lanes per time point, two library prep reactions were carried out; one library prep for the single cell transcriptome and one generating a paired MultiSeq library. Reagents were thawed and stored on ice. Dynabeads cleanup mix, Elution solution I and cDNA amplification mix were prepared as described in table 1. 10mL of 80% ethanol was freshly prepared. On ice, amplification mixture was combined with

barcodes by adding 50uL cDNA amplification mix, 15uL of cDNA primers (from 10x) and 1uL of MultiSeq primer (from IDT) to each of six wells in a strip tube. 125uL of recovery solution was added to each first strand synthesis reaction from day 1 and incubated at room temperature. The pink layer was removed and discarded from the biphasic solution. Dynabeads solution was vortexed and 200uL was added to each recovered reaction. Mixing occurred by pipetting up and down ten times. Sample was bound to beads by incubating 10 minutes at room temperature with pipette mixing half way through. Dynabeads were cleaned up on a 10x magnet by first binding beads to magnet, removing and discarding supernatant, washing two times with 300uL 80% ethanol and then spinning to collect remaining ethanol at the bottom which was then removed with beads bound to magnet. Samples were then air dried for 1 minute. To elute, the sample was resuspended in 34.5uL of elution solution I, incubated for 2 minutes, and then separated from beads on the magnet. 34uL of clear solution was

transferred to the cDNA amplification strip tube. Strip tube was placed in the thermal cycler and the Library Amplification (table 2) protocol was run. After amplification the two libraries were cleaned up and separated using SPRI beads. 60uL of SPRI beads were added to each 100uL amplification reaction and then incubated at room temperature for five minutes. The SPRI beads were immobilized using the magnet and then the supernatant fraction was saved in 1.5mL tubes (CRITICAL this contains the barcode library). Continuing with the cDNA library, the beads were washed two more times using 200uL, 80% ethanol. Excess ethanol was removed by spinning and aspirating prior to drying for 2 minutes at room temperature. The sample was resuspended in 40.5uL of Qiagen elution buffer and separated from the beads on the magnet. 40uL of the cDNA library was transferred to fresh PCR tubes. Continuing with the barcode sample saved from before, 260uL of SPRI beads and 180uL of isopropanol was added to the 60uL supernatant volume. The sample was

incubated for five minutes to precipitate the sample on the beads and then separated on the magnet until clear. The supernatant was discarded and the beads were washed two times in 500uL, 80% ethanol. Excess ethanol was removed via centrifugation, aspiration and air drying 2 minutes as before and the MultiSeq Barcode Libraries were eluted using 50uL Qiagen elution buffer.

Barcode Library Prep

Qubit quantification of samples was performed using 1uL of MultiSeq barcode libraries. Barcode Amplification Mix was prepared (table 1) in each of 6 strip tube wells making sure to record barcode/sample associations. The strip tube was transferred to the thermal cycler and incubated using the Barcode Library Amplification program (table 2). After the amplification program was completed, samples were cleaned up using SPRI beads. This was done as before by adding 80uL of

SPRI beads to each reaction, incubating 5 minutes, and washing on the magnet two times with 200uL of fresh 80% ethanol. Excess ethanol was removed via centrifugation, aspiration and air drying 2 minutes as before and the MultiSeq Barcode Libraries were eluted using 25uL Qiagen elution buffer.

Assessing Quality and Quantity of Samples

All samples (6 single cell cDNA molecules, 6 single cell RNAseq libraries and 6 matched single cell barcode samples at each time point) were assessed for quantity using the Qubit High Sensitivity DNA assay and quality using the Agilent Bioanalyzer High Sensitivity kit. Quality was estimated by interpreting the electropherograms from the Bioanalyzer to determine if the distribution of molecule sizes

Table 2: Thermal Cycling Protocols		
Library Amplification		
1	98C	3 min
2	98C	15 sec
3	63C	20 sec
4	72C	1 min
5	Go to step 2	11 additional cycles (12 total)
6	72C	1 min
7	10C	hold
Barcode Library Amplification		
1	95C	5 min
2	98C	15 sec

3	60C	30 sec
4	72C	30 sec
5	Return to step 2	9 times (10 total cycles)
6	72C	1 min
7	10C	hold

approximated expected values and that there was not significant material from other fragment sizes (representing amplified oligonucleotides and oligonucleotide dimers). Samples with sufficient material of high quality were chosen to be proceeded with.

Single Cell RNAseq Nextera Library Prep

cDNA was transformed into sequencing libraries using the Nextera HT kit from Illumina.

Individual time point analysis

For primary analysis, each individual timepoint was first analyzed separately. MULTI-Seq count matrices were aggregated per timepoint (joining all replicates/genotypes for a given timepoint) and loaded using the Scanpy package into an AnnData object (Cf. Scanpy documentation). We refer to a given timepoint as a dataset in the following paragraph.

For preprocessing and data visualization, the different datasets were analyzed using the Scanpy package. Briefly, genes expressed in less than 3 cells were filtered. For week 2 data, cells with less than 700 expressed genes were removed. For the rest of the timepoints, the threshold was set at 200 genes. Cells with more than 10% mitochondrial transcripts were removed. Counts per cell were normalized for library size (library size = 1e4) and log-transformed. The top highly variable genes were selected using the following parameters: min_mean=0.0125, max_mean=3,

min_disp=0.5. PCA was performed, retaining the top 25 principal components (PCs) by explained variance. For 2D data visualization, a k-nearest neighbor (k-NN) graph was computed in PC-space, using k=10. The UMAP algorithm was used to compute a 2-dimensional embedding of cells. Clustering of cells was performed using the Louvain community detection algorithm on the k-NN graph previously computed, using a default resolution of 1.

For cell type annotation in individual timepoints, differential gene expression was performed in a "1-vs-rest" fashion across Louvain clusters. Briefly, a Wilcoxon rank sum test was performed on log-transformed data to rank genes for each cluster. Finally, functional annotation of cell types was performed looking at the top 200 genes per cluster. Visual exploration was performed using the CellBrowser, in order to refine annotation by grouping similar clusters together.

Aggregated dataset analysis

Once each cell type was annotated in the individual timepoints, we performed an aggregated analysis of all timepoints. Raw count matrices were combined and the following analysis was performed. For preprocessing and data visualization, the different datasets were aggregated and analyzed using the Scanpy package. For the filtering, genes expressed in less than 3 cells were filtered. Cells were filtered to retain those that were retained in the individual timepoint analysis. Cell type labels were then transferred from the individual timepoint datasets. The rest of the analysis (normalization, 2D visualization of aggregated data) was performed as described for the individual timepoints. Categorical enrichment of cell types in a particular timepoint/genotype was performed using a hypergeometric test as implemented in the Scipy package.

Trajectory analysis

For trajectory analysis, we used Monocle3. Trajectory were computed using normalized count data from the individual timepoints as well as the aggregated dataset. Scnapy normalized data were exported and loaded to R into a CDS object. Default parameters were used following the Monocle3 tutorial found here. Briefly, the preprocessing step was skipped, and we used Monocle3 dimensionality reduction method as well pseudotime computation with default parameters.

Chapter 2

Organoid Platform Engineering

Introduction

This chapter was adapted from Seiler, Mantalas et al. “Modular automated microfluidic cell culture platform reduces glycolytic stress in cerebral cortex organoids” Nature Scientific Reports 2022. My personal contribution to this was in the idea of the autoculture system, the experimental plan, and carrying out the experiments.

Background

Cell culture has been a principal model for studying human disease and development for over 70 years since the isolation of HeLa cells from a human cervical cancer biopsy[13,14]. Originally used as a vehicle to research viruses, human cell culture protocols were optimized for quick and easy growth to produce large quantities of material. While tissue culture protocols have

advanced, particularly in reducing many media components, much of these original recipes remain in place. There is still much room to improve for tissue culture protocols to mimic physiological nutrient concentrations, supply, and removal. Automated microfluidics allows us to move beyond traditional protocols by feeding at rates and precision not manually feasible.

Recent advances in stem cell and developmental biology have generated more accurate models resembling aspects of primary human tissue[15,16]. Human embryonic stem (hES) cells and induced pluripotent stem (iPS) cells, collectively referred to as pluripotent stem cells (PSCs), have the potential to differentiate into most cell types of the body, and protocols capitalized upon this to generate 3D culture models for human tissues including brain, gut, liver and breast[17,18]. These self-assembling, organ-specific cell cultures, called organoids, are broadly utilized as *in-vitro* models in

developmental research, pathogenesis, and medicine[19–21]. Organoids mimic key functional characteristics of their primary tissue counterpart's physiology more accurately than 2D cell

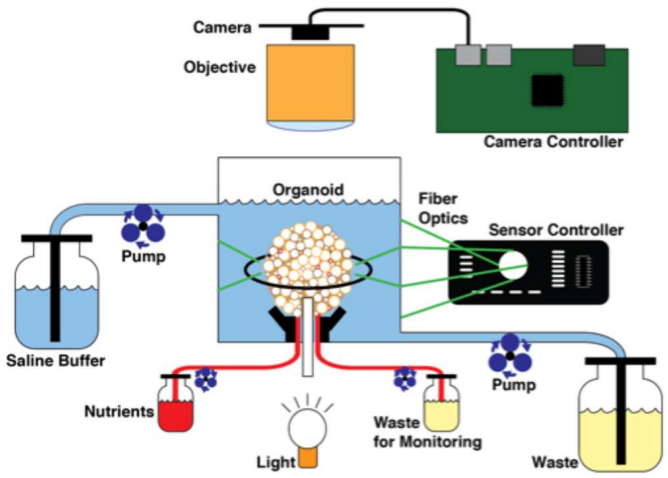

cultures[18]. Beyond use as *in-vitro* models, organoids are also being explored for applications in regenerative medicine, and healthcare as tissue for implants[17]. As the technology opens up new frontiers, there is a raising need for better methods to grow, control, and analyze organoid cultures. There is a need to lessen the gap between in-vitro cultures and primary tissue. Efforts like the advances shown here leverage precision microfluidics, robotic automation, and contact-less sensing to enable

robust, reproducible cell culture optimized for tissue fidelity.

The ability of PSC-derived organoids to self-assemble and generate many tissue-specific cell types makes them particularly useful for modeling complex tissues and systems. The brain contains some of the highest complexity in the human body, and researchers can generate high-quality models of different brain regions with organoid technology. Cerebral organoids are a form of brain organoid that models the physiology of the cerebral cortex, containing many cortex-specific cell types and sub-regions[22]. These organoids are widely used for research on prenatal brain development[23-25], brain pathologies[26], and therapeutic testing[27]. Cerebral organoids will grow to a few millimeters in diameter during prolonged culture and can be maintained in culture indefinitely[28].

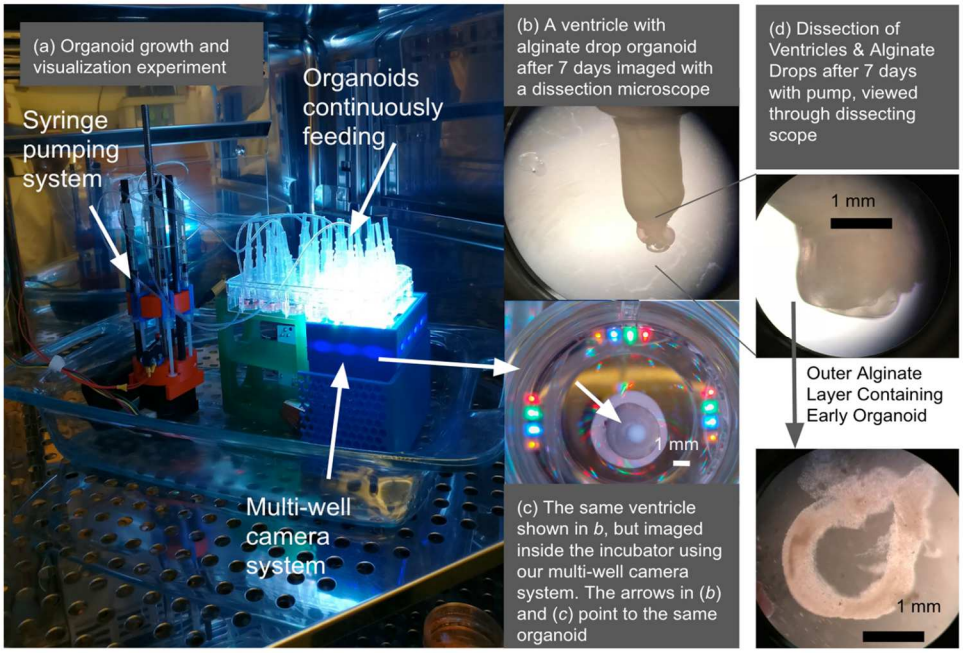

Key components to engineering an automated organoid culturing platform include reagent reservoir(s), waste reservoir(s), pumps to control flow, physical substrate to hold the organoid, and monitoring systems (figure 11) all in standard incubator conditions. Here we describe the iterations that we went through in developing the Autoculture system, starting with a proof of concept system shown in figure 12 with a hanging ceramic substrate, and concluding by demonstrating more physiological gene expression when using the Autoculture system for culture.

Results

Utilizing internal feeding points from a hanging substrate resulted in disruption to the tissue (figure 12), so we shifted our focus towards a flow channel above an organoid cavity (Figure 13A). The idea was to minimize turbulence localized to the organoid by maintaining consistent flow channel geometry over the cavity. This was done by including a hydrogel scaffolding around the organoid, filling the cavity to the level of the flow channel. Trapped air and complete removal of old media were of great concern, so we used the loading port as an air exhaust allowing for excess pumping volume to be used in both the fill and aspiration (Figure 13B). After several iterations we had a stable build that maintained living tissue through multiple days of feeding (figure 13C). This was the prototype Autoculture system.

Figure 14 illustrates the process of generating human cerebral organoids by aggregating human

PSCs[5,29]. Neural induction is achieved by inhibiting the WNT (IWR1-ε) and Nodal/Activin (SB431542) pathways that yield both dorsal and ventral cortical tissue. As organoid development proceeds at a pace similar to primary fetal development, these cultures must be maintained for weeks to months to observe late-stage cell types and tissue structures. These include terminally differentiated cell types such as neurons, astrocytes, and oligodendrocytes, and the observation of locally-organized rosettes comprised of radial glia neural stem cells (Figure 14B). Current protocols of cerebral organoids have limitations in throughput, consistency, and reliability, as well as impaired health, showing hallmarks signs of cellular stress[6,30]. The phenotype of cell stress is likely multifactorial; however, many factors may result from traditional cell culture. The pace of manual media changes (often once every 1-3 days) leads to erratic swings in nutrient availability and the build-up of toxic metabolites. By feeding

outside the incubator, cells experience colder temperatures and reduced dissolved carbon dioxide leading to a more alkaline environment. Lab automation is becoming increasingly prevalent in life sciences to reduce the effect of these uncontrolled variables and increase the quantity and quality of experiments enabling easy long-term maintenance with minimal manual requirements.

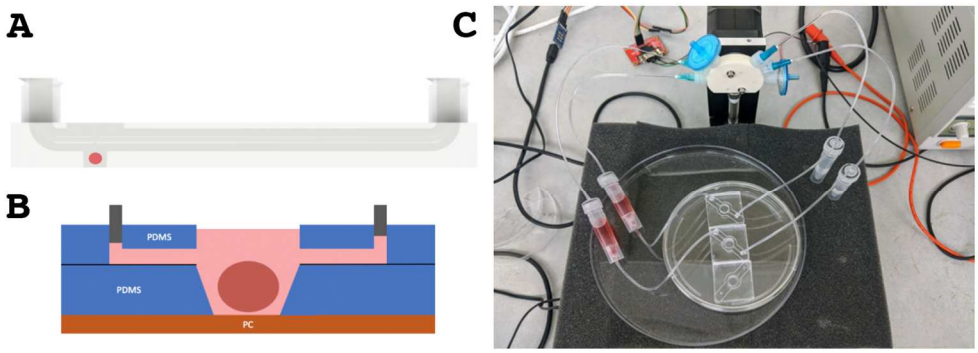

Figure 13: Early iterations of the Autoculture system. *(A)Computer aided design rendering of 3D printed version of disposable chip. (B) Drawing of early manufacturing design for PDMS chip. (C) Working build testing flow delivery using Tecan pump.*

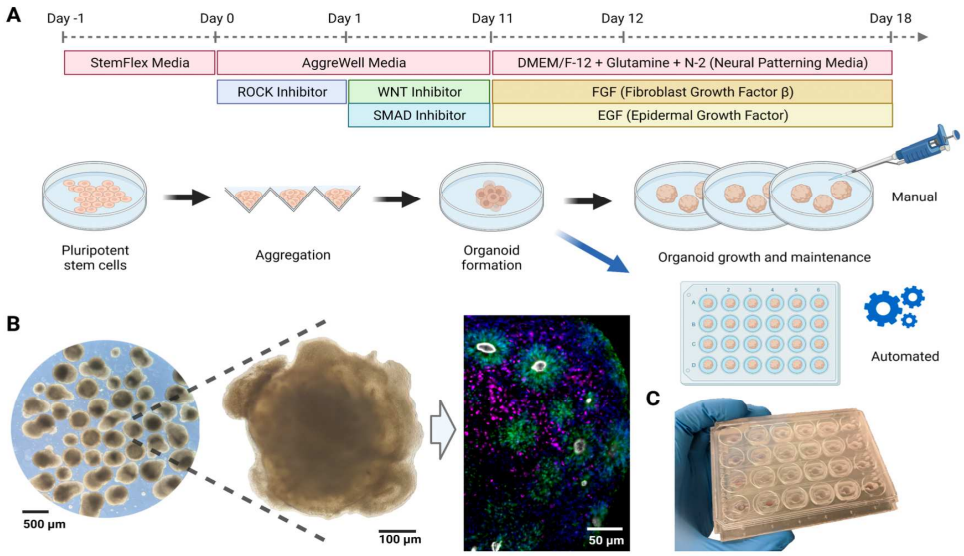

Figure 14. Overview of the human cerebral organoid generation protocol. *(A) Human pluripotent stem cells are expanded in traditional 2D culture, dissociated, aggregated into microwells, and matured into 3D organoid cultures using defined media conditions to promote cerebral cortex tissue differentiation. In this study, on day 12 post-aggregation, organoids were either kept in suspension and maintained manually (black arrow) or transferred to individual wells of a microfluidic chip and maintained in automation (blue arrow). (B) Images of cerebral organoid cultures. Bright-field images at low (left) and high (center) magnification under standard culture conditions show organoid morphology and heterogeneity. Immunofluorescence stains on week 5 for PAX6 (green, radial glia progenitor cells), CTIP2 (BCL11B) (magenta, excitatory projection neurons), ZO-1 (TJP1) (white, tight junction proteins on radial glia endfeet, apical surface of the neural tube), show characteristic ventricular zone-like*

rosette structures with radial glia surrounded by neurons. Nuclei stained with DAPI (blue). (C) Image of the PDMS microfluidic chip. The custom cell culture chip, modeled after a standard 24-well plate, houses organoids for automated experiments.

The Autoculture Platform

We developed an automated, microfluidic cell culture platform to optimize 3D organoid growth, the "Autoculture" platform. The system consists of six linked modules (Figure 15): (1) Refrigerator with reagent reservoirs (e.g., fresh media), (2) Syringe pump, distribution valves, and control interface, (3) conditioned media collection reservoirs in cold storage, (4) a microfluidic serial bus interfacing with a cell culture incubator, and (5) a multiplexed microfluidic organoid chip that (6) immobilizes organoids within their micro-environment vessel (1 of 24 wells). To feed the organoids, each

individual well is serviced by a fluidic controller; the controller removes spent media via aspiration to a collector in cold storage and then replenishes the vessel with fresh media at programmable intervals.

Each of the 24 wells of this system is a separate, isolated experiment with a dedicated inlet tube, outlet tube, and collection reservoir. Each well's feeding schedule is fully customizable in rate and media to increase the flexibility of experimentation. A range of 5–1000 µL aliquots from 3 media/reagent reservoirs can be scheduled to any well. Media/reagent reservoirs may also be used in combination. By design, each well forms a fluidic circuit that maintains isolation from the other circuits on the plate (See Methods). A full 24-well plate is serviced in 72 seconds, and the time between fluid injections may be any length beyond (for instance, every hour, twice a day, every other day, etc.). Conditioned media may be retrieved for molecular analysis without

disrupting the culture at any point during or after the experiment. After the experiment, the organoids are retrieved for molecular analysis.

With these control parameters, entire plates may carry out the same workflow to generate consistent batches of organoids. One can also titrate a reagent with an incremental gradient in concentration from well 1 to 24. In addition, one can run multiple protocols/feeding schedules across the plate and change the media components or feeding schedules at various time points throughout an experiment.

Microfluidic Organoid Chip

Figure 16 describes the manufacturing and assembly process of the PDMS microfluidic chip. The optically-transparent glass- PDMS microfluidic chip has the footprint of a 24-well plate (85.5 mm x 127.6 mm) to integrate with laboratory tools such as microscopes, plate readers, and robotic dispensers. The 24 isolated wells are addressable via 2 mm square channels at

the glass–PDMS interface. For convenient accessibility, all inlets are located in a row on the edge of the chip's face and all outlets are located in a row on the opposing edge. The open-loop design here is observed with wells that are open to the air. This way, bubbles accumulated in the system are exhausted, there is free gas exchange with the incubator environment, and organoids are easily accessed during chip loading and the experimental conclusion. Each well traps 120 µL that can be used as a micro-environment, including the use of extracellular scaffolds.

Each 3D-printed, fluidic interface plate simultaneously connects 24 inlet tubes to the inlets/outlets of the microfluidic chip. Three bores seal the Tygon tubing about the rigid projections. The collection of 24 lines mates with the molded holes in the PDMS, creating a bore seal with all tubes.

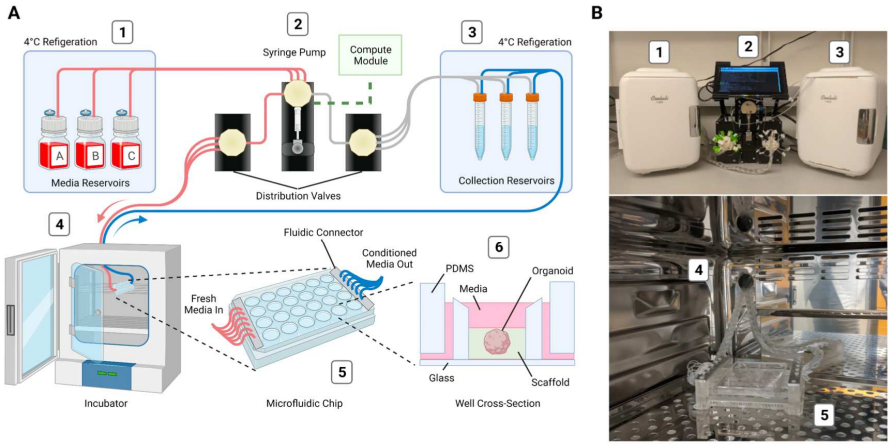
A
1
4°C Refigeration
A
B
C
Media Reservoirs
2
Syringe Pump
Compute Module
Distribution Valves
3
4°C Refigeration
Collection Reservoirs
4
Incubator
Fluidic Connector
Conditioned Media Out
Fresh Media In
5
Microfluidic Chip
6
PDMS
Media
Organoid
Glass
Scaffold
Well Cross-Section
B
1
2
3
4
5

Figure 15. Design and implementation of the automated, microfluidic culture platform. *(A) Illustration of the automated, microfluidic organoid culture platform, the Autoculture. (B) Front view images of the Autoculture. (1) Refrigerator with reagent reservoirs. (2) Syringe pump, distribution valves, and control interface. (3) Refrigerator with conditioned media collection reservoirs. These components reside on a lab bench directly above the cell culture incubator. (4) Microfluidic tubes enter through an incubator port and connect to the (5) microfluidic well plate chip inside the incubator. (6) Cross-sectional diagram of a single well containing an organoid culture.*

Culture of Cerebral Organoids

The growth of cerebral organoids on Autoculture was compared to that of orbital shaker conditions in an 18-day experiment. Human pluripotent stem cells were aggregated to form organoids and maintained under standard conditions for the first 12 days during neural induction (see Methods). The batch was split, and 12 organoids were loaded onto an Autoculture microfluidic chip while the remainder were maintained in a 6-well plate on an orbital shaker as controls.

Each automated organoid was fed 70 µL every hour for six days, while the controls were fed 2 mL every other day. In automation, the well plate does not need to be periodically removed from the incubator for feeding; therefore, this system is well-suited for longitudinal monitoring of organoid development. In this study, organoids in the Autoculture well plate were monitored once per hour using a bright-field imaging in-incubator platform[31,32].

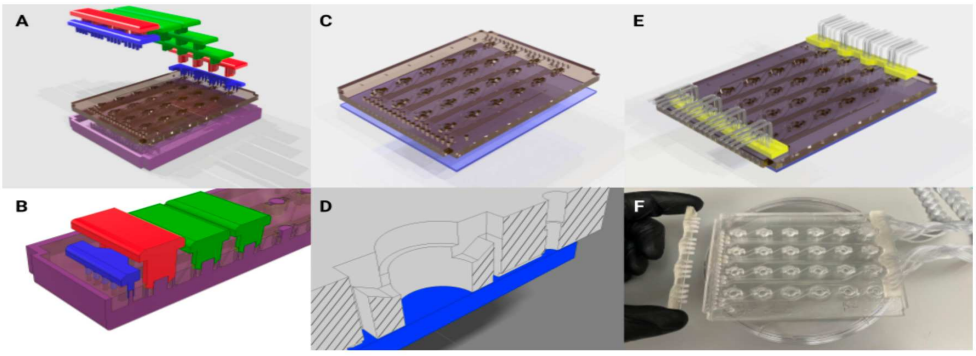

Figure 16. Fabrication of the PDMS microfluidic chip. *(A) Graphical rendering of the interlocking mold pattern for the PDMS substrate in the microfluidic chip assembly. (B) Interlocking mounts (blue, red, and green) affix to the base mold (purple) and define microfluidic geometries upon the poured PDMS that are retained as the substrate cures. (C) The PDMS substrate is removed from the mold and bonded to glass. (D) A cross-sectional rendering of the chip. Fluid enters from microfluidic inlets on the surface and follows channels sealed by glass on the bottom to wells with open access from the top. (E) A 3D-printed fluidic interface*

plate (yellow) connects 24 fluidic microtube lines with the inlets/outlets of the microfluidic chip. (F) Microfluidic chip (center) with an example of the fluidic interface plate (left) and fully installed fluidic interface plate (right).

Live Imaging

Figure 17A shows the automated, microfluidic culture plate inside an incubator placed on a remote-controlled, IoT-enabled, multi-well automated imaging system. The imaging system was designed to monitor biological experiments in a 24-well plate format, using one dedicated camera for each well. To account for the three-dimensional development of the organoids during the entire experiment, we captured bursts of images, sweeping through the range of focal distances covering the entire three-dimensional tissue. A computer vision algorithm was used to detect the features in focus at each focal plane, generate a composite image maximizing the in-

focus features in the entire organoid, and compute the projected area. This process is described in previous work[32]. Figure 17B shows 12 cerebral cortex organoid cultures (day 12), loaded in individual wells of the microfluidic chip and fed in parallel on the Autoculture platform for the experiment. Figure 17C and D show the growth of "Culture 4" over six successive days. Robust organoid growth was observed for the organoids in the Autoculture wells and was consistent with the size increase observed for the organoids grown under control conditions. Compared to controls, automated organoids did develop a less-dense perimeter, suggesting that the reduction in velocities and shear forces may accommodate growth and migration that would otherwise be cleaved.

Growth Analysis

On day 18, the cultures were harvested and analyzed by bulk RNA sequencing (RNA-seq) and immunohistochemistry to evaluate the cell types

generated in each condition and the overall health of the cell cultures. The transcriptomes of 7 “Automated” and 4 “Suspension” organoids were compared. Gene expression of cell-type markers for neuralepithelia (SOX2), radial glia neural stem cells (SOX2, HES5, PAX6, HOPX), intermediate progenitors (EOMES), and immature neurons (NeuroD1, RELN) did not show consistent differences between the Autoculture and control samples suggesting that overall differentiation fidelity was not affected by using the Autoculture system. Consistent with this, we saw a robust expression of the neural progenitor protein markers, SOX2 and Nestin by immunohistochemistry in sections of organoids grown under standard or Autoculture conditions (Figure 18B).

Contrasting automated and control organoids, we observed a significant difference in the expression of genes associated with cell culture stress. Studies have shown that glycolysis and endoplasmic reticulum stress (ER stress) pathways

are upregulated in organoids relative to in vivo tissue samples, and these correlate with impaired cell subtype specification and maturation[5,33]. In this study, canonical glycolysis was the top deferential pathway with the vast majority of the significant genes consistently downregulated. Genes that are notably upregulated in cerebral organoids showed reduced levels in the automation condition: ALDOA, ENO1, HK1, and PGK1 had fold changes of −6.9, −10.4, −2.8, and −9.3, respectively (Figure 18A). Additionally,

markers of ER stress: ARCN1, GORASP2, and YIPF1 were reduced by fold changes of −2.8, −2.2, and −3.0, respectively.

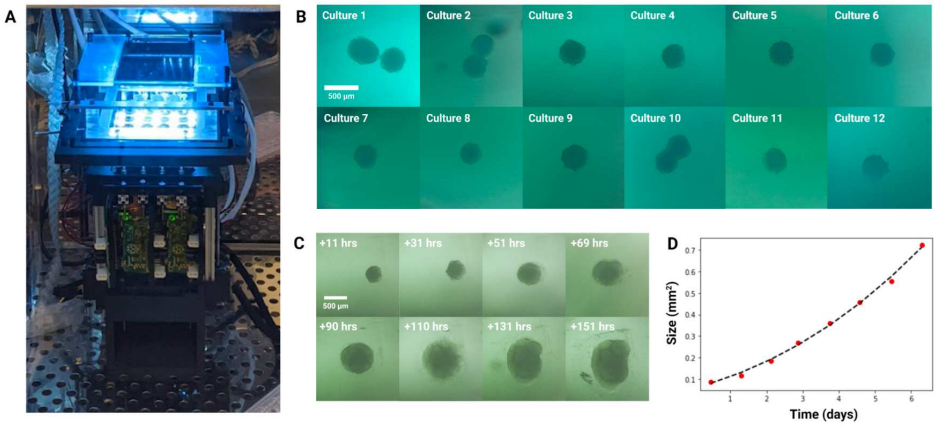

Figure 17. Longitudinal monitoring of organoid development. *(A) The Autoculture microfluidic chip sits on a remote-controlled, IoT-enabled, 24-well automated imaging system. (B) Bright-field images of twelve individual 12-day-old cerebral cortex cultures at day 1 of automated feeding. (C) Longitudinal imaging of "Culture 4" during the experiment. (D) Projected area expansion of "Culture 4" during the experiment. This was obtained using a computer vision algorithm34.*

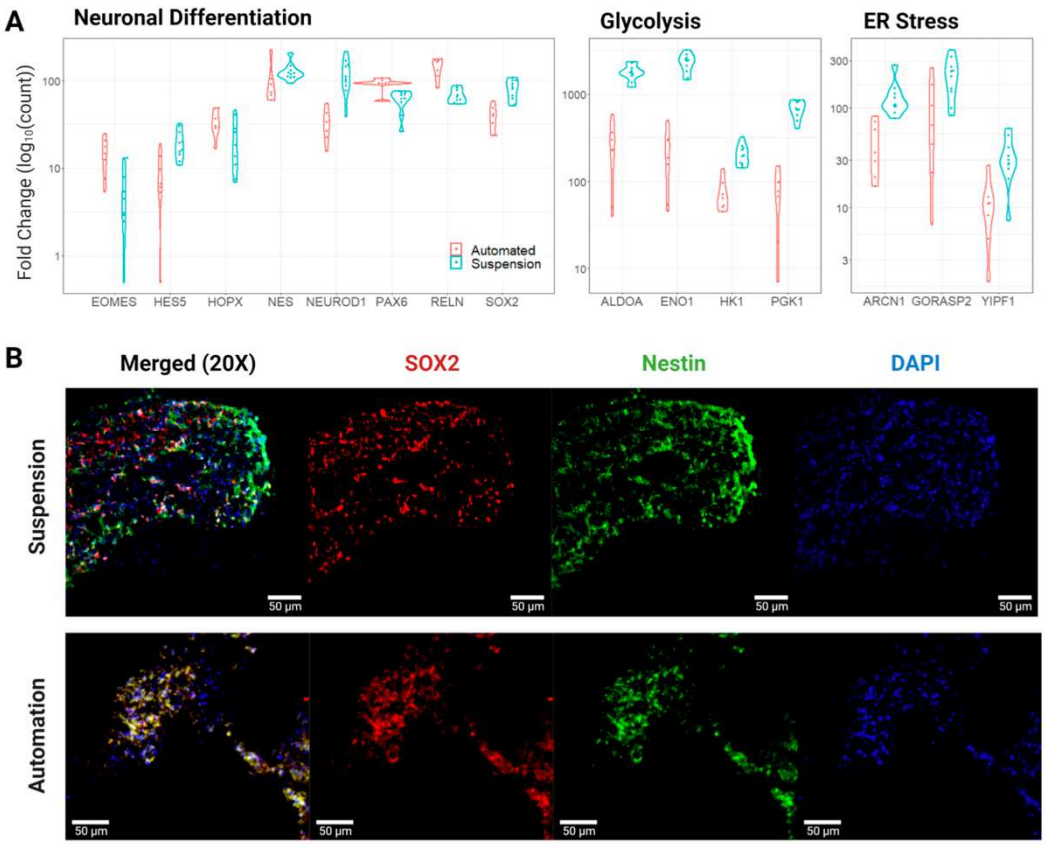
A
Neuronal Differentiation
Glycolysis
ER Stress
Fold Change (log10(count))
Automated
Suspension
EOMES
HES5
HOPX
NES
NEUROD1
PAX6
RELN
SOX2
ALDOA
ENO1
HK1
PGK1
ARCN1
GORASP2
YIPF1
B
Merged (20X)
SOX2
Nestin
DAPI
Suspension
Automation
50 µm

Conclusions

The increasing demands for long-term experiments, reproducibility, parallelization, and longitudinal analysis drive cell culture toward automation. This study showcases an automated, microfluidic solution for the growth and maintenance of organoids capable of existing in conjunction with other control and sensing devices over the Internet of Things, magnifying the ability to capitalize on the precision robotics for automated experimentation. Combining this platform with the imaging platform provides a stationary environment that uniquely enables the live study of individual organoids over time.

Reducing stress levels in cerebral organoid models is crucial to achieving physiological relevance. As measured by reduced glycolytic enzyme expression, the environment of the Autoculture platform results in reduced-stress organoids compared to traditional suspension culture conditions. Pathways that respond to

environmental conditions such as sugar metabolism, hypoxia monitoring, and protein production are interconnected through the integrated stress response pathway. By reducing concentration fluctuations in the cell culture media through automated feeding, the cultures may experience greater homeostasis. Further investigation is needed to understand the potential long-term effects of reducing gene expression of glycolysis and ER stress genes and the critical environmental conditions that underlie the gene expression signature associated with less cell stress we observed. For example, it is unclear whether depletion of essential nutrients, like glucose, or accumulation of cell metabolites, like lactose, is the critical factor leading to the induction of genes in the glycolysis pathway observed under standard organoid culture conditions. However, the Autoculture system we developed here provides a platform in which we can systematically explore this question.

Methods

Design of the Autoculture platform

Cell culture media was stored in glass bottle reservoirs (Corning) with a multi-port solvent delivery cap (Spex VapLock) and stored at 4°C for the duration of the experiment. Each reservoir delivery cap contained a single 0.030” ID x 0.090” OD Tygon microbore tube (Masterflex), sealed by a two-piece PTFE nut and ferrule threaded adapter (Spex VapLock), extending from the bottom of the reservoir to an inlet port on the 6-port ceramic valve head of the syringe pump (Tecan Cavro Centris, 1.0-mL glass vial). Sterile air is permitted to backfill the reservoir through a 0.22-µm filter (Millipore) affixed to the cap to compensate for syringe pump reagent draws. The same Tygon microbore tubing and PTFE nut and ferrule threaded adapters were used to connect the syringe pump to two parallel 12-port distribution valves (Tecan SmartValve). Each 0.020” ID x 0.060” OD Tygon microbore tube

(Masterflex) emanating from the distribution valve connects to a single well of the microfluidic chip. Fluidic isolation between wells is retained from this junction onward. Each 12-port distribution valve services six wells on the microfluidic chip. Systems with two and four distribution valves were constructed. The collection of 2-meter long microbore tubes was bundled into a braid for convenient handling and guided through the rear entry port of a standard cell culture incubator (Panasonic) (Figure 14(4)). At incubator conditions (37°C, 5% CO2, 95% rel. humidity), a single custom, 3D-printed fluidic interface plate mated the set of microbore tubes for reagent delivery to the inlets of the microfluidic chip and a second, identical interface plate mated the set of microbore tubes for reagent aspiration to the outlets.

The microbore tubes for aspiration were guided back out of the incubator and to a set of single-use 15-mL conical tubes (Falcon) for conditioned

media collection (Figure 14(3)). Each collection reservoir was capped with a rubber stopper (McMaster) containing two 0.06” drilled holes. For each stopper, the microbore tube sourcing conditioned media from the microfluidic chip was inserted into one hole, and a dry microbore tube for pneumatic operation routes back to the aspiration distribution valve head was inserted into the other hole. The syringe pump was used to generate negative pressure upon each collection reservoir in series to draw conditioned media from the microfluidic chip into the collection reservoir. The separation between the pneumatic tube and conditioned media tube trapped the influx of media in the collection reservoir. All microbore tubes were hermetically sealed to the distribution valve and syringe pump with PTFE nut and ferrule threaded adapters.

The syringe pump and distribution valves were connected using the multi-pump electrical wiring configuration described in the Tecan manual. A

compute module (Raspberry Pi 4) relayed serial communications with Tecan OEM Communication Protocol using a GPIO TX/RX to DB9M RS232 serial expansion board for Raspberry Pi (Ableconn). The Raspberry Pi compute module used a 7” touchscreen display to edit and launch protocols. An open-source Python application program interface (API) was used to develop the software required to carry out protocols in automation29.

PDMS Molding

PDMS-based microfluidics were constructed using an interlocking 3D-printed plastic mold (Figure 15). These were printed with an SLA printer (Formlabs Form 3) with Model V2 resin. The printed molds were post-processed with sonication in isopropanol (IPA) for 20 minutes to remove excess resin, followed by drying in N2. Dry components were cured under UV-light (405nm) for 30 minutes at 60°C. As illustrated in Figure 16A, the mold parts were assembled and filled with PDMS (Sylgard

184, Dow Corning) prepared by mixing PDMS prepolymer and a curing agent (10:1 w/w). After filling the mold, the PDMS was degassed in a vacuum chamber for 1 hour. The PDMS-filled mold is left to cure for 24 hours at 60°C before removal of the PDMS from the mold.

Microfluidic Chip Assembly

Borosilicate glass substrates (101.6mm x 127.0mm, McMaster-Carr) were cleaned via sonication in acetone (10 minutes), then isopropyl alcohol (10 minutes), and dried with N2. The glass substrate and molded-PDMS surface were activated with oxygen plasma at 50W for 45 seconds. The glass and PDMS (Figure 16C) were aligned by hand, pressed together, and baked at 100°C on a hot plate for 30 minutes, forming an irreversible seal.

Parylene Coating

A 10 µm layer of parylene-C (Specialty Coating Systems) was deposited onto the microfluidic chip to prevent PDMS absorption of small molecules. Two drops of silane A-174 (Sigma-Aldrich) were loaded into the deposition chamber to promote adhesion.

3D Printed Components

The fluidic interface plate (Figure 16F) was 3D printed to interface the 2.2 mm OD microbore tubing (Cole-Palmer) with the PDMS inlet and outlet features. Each connector geometry consisted of 24 cylindrical extrusions with an OD of 2.7 mm and a bore of 2.2 mm. Within each bore were three 0.2 mm long barbs to grip the microbore tubing when inserted. This component was printed with a Formlabs SLA printer (Form 2) with Surgical Guide resin with sonication in isopropanol (IPA) for 20 minutes to remove excess resin, followed

by drying in N2. Dry components were then cured under UV light (405 nm) for 30 minutes at 60°C. To ensure biocompatibility, the part was coated with 5 µm of parylene-C (Specialty Coating Systems). Two drops of silane A-174 (Sigma-Aldrich) were also loaded in the deposition chamber with the device to promote adhesion.

Sterilization

Sterilization of the syringe pump, valve heads, tubing, fluidic interface plates, and collection tube caps was carried out per supplier recommendation (Tecan). A 10-minute wash with 70% ethanol sourced from an autoclaved glass reservoir was pushed through the platform to the collection reservoirs via the syringe pump. Following 70% ethanol, a drying cycle of sterile air sourced through a 0.22 µm filter (Millipore) was applied for 10 minutes. Ten subsequent cycles of deionized, nucleus-free water and drying were carried out under the same parameters. The

microfluidic chip and media reservoirs were autoclaved at 121°C for 45 minutes and dried for 15 minutes immediately prior to use. All components were transferred via sealed autoclavable bags to a biosafety cabinet in tissue culture for organoid and media loading. Pre-prepared, supplemented media was transferred to each media reservoir and capped (VapLock) and then stored in refrigeration for the duration of the experiment.

hESC line maintenance

The human embryonic stem cell line H9 (WiCell, authenticated at source) was grown on recombinant human vitronectin (Thermo) coated cell culture dishes in StemFlex Medium (Gibco). Subculturing was performed by incubating plates with 0.5 mM EDTA for 5 minutes and then resuspended in culture medium to be transferred to new coated plates.

Cerebral organoid differentiation and protocol

To generate cerebral organoids, adherent cultures were dissociated into single cells using Accutase Cell Dissociation Reagent (Gibco) and then aggregated in AggreWell 800 24-well plates (STEMCELL Technologies) at a density of 3,000,000 cells per well with 2mL of AggreWell Medium (STEMCELL Technologies) supplemented with Rho Kinase Inhibitor (Y-27632, 10 µM, Tocris, 1254) (day 0). The following day (day 1), 1mL of the AggreWell medium was manually replaced with supplemented medium containing WNT inhibitor (IWR1-ε, 3 µM, Cayman Chemical, 13659, days 1-10) and Nodal/Activin inhibitor (SB431542, Tocris, 1614, 5 µM, days 1-10). On day 2, aggregates were transferred onto a 37 µm filter (STEMCELL Technologies) by carefully aspirating with a p1000 wide-bore pipette out of the AggreWell plate. The organoids were transferred into ultra-low adhesion 6-well plates (Corning) by inversion and rinsing of the filters with fresh AggreWell

medium. Media was changed on days 3, 4, 5, 6, 8, and 10 by manually replacing 2 mL of conditioned media with fresh media. On day 11 and onward, the medium was changed to Neuronal Differentiation Medium containing Eagle Medium: Nutrient Mixture F-12 with GlutaMAX supplement (DMEM/F12, Thermo Fisher Scientific, 10565018), 1X N-2 Supplement (Thermo Fisher Scientific, 17502048), 1X Chemically Defined Lipid Concentrate (Thermo Fisher Scientific, 11905031) and 100 U/mL Penicillin/Streptomycin supplemented with 0.1% recombinant human Fibroblast Growth Factor b (Alamone F-170) and 0.1% recombinant human Epidermal Growth Factor (RD systems 236-EG).

Control-group "Suspension" organoids remained suspended in 6-well plates and were maintained with 2 mL media changes every other day for the remainder of the culture. Experimental-group "Automated" organoids were loaded onto the microfluidic chip and experienced media changes

of 70 µL once every hour for the remainder of the culture.

Microfluidic chip loading

On day 12 of cerebral organoid differentiation, the microfluidic chip was prepared by pipetting 50 µL of chilled (approximately 0°C) Matrigel hESC Qualif Matrix (BD 354277) into each well. Immediately following Matrigel, single cerebral organoids were transferred via p1000 wide-bore pipette with 70 µL of native conditioned media to each well and positioned to center-well for imaging. The chip was covered with a 24-well plate lid and incubated at 37°C for 15 minutes to set the Matrigel. Each well was filled with an additional 70 µL of fresh media and connected to fluidic interface plates (Figure 16F) routed into the incubator through a rear access port. The fluidic interface plates were pressure fitted into the microfluidic chip by hand, and the chip

was positioned on the imaging platform (if applicable).

Sequencing library preparation

Smart-seq2 protocol[34] was used to generate full-length cDNA sequencing libraries from whole organoid mRNA. Briefly, whole organoids were lysed using lysis buffer to render cell lysate containing polyadenylated mRNAs that were reverse transcribed with Superscript III (ThermoFisher Scientific) using an oligoDT primer (/5Me-isodC/AAGCAGTGGTATCAACGCAGA GTACTTTTTTTTTTTTTTTTTTTTTTTTTTTTVN) and template switching was performed with a template switch oligo (AAGCAGTGGTATCAACGCAGAGTACATrGrGrG). The oligoDT primer and template switch oligo sequences served as primer sites for downstream cDNA amplification (AAGCAGTGGTATCAACGCAGAGT). cDNA was quantified using a Qubit 3.0 DNA high sensitivity fluorometric assay, and quality was assessed

using a bioanalyzer DNA high sensitivity kit (Agilent). Nextera HT transposase (Illumina) was used to convert 1 ng of cDNA into barcoded sequencing libraries.

Transcriptome analysis

Paired-end reads were sequenced at 75x75 bp on an Illumina NextSeq 550, and further depth was sequenced at 50x50 bp on an Illumina NovaSeq 6000 to an average read depth of 65 million paired reads per sample. Samples were demultiplexed using Illumina i5 and i7 barcodes, and higher depth samples were sub-sampled to 100M using SAMtools[35]. Trimmed reads were combined and aligned to the human genome (hg38 UCSC assembly) with STAR alignment[36] (Gencode v37) using the toil-rnaseq pipeline[37]. STAR parameters came from ENCODE's DCC pipeline41. Differential gene expression was performed using the DESeq2[39] package in RStudio. Gene set enrichment analysis was performed using g:Profiler[40].

Immunostaining

Cerebral organoids were collected, fixed in 4% paraformaldehyde (ThermoFisher Scientific 28908), washed with 1X PBS and submerged in a 30% sucrose (Millipore Sigma #S8501) in PBS solution until saturated. Samples were embedded in cryomolds (Sakura – Tissue-Tek Cryomold) containing tissue freezing medium (General Data, TFM-C), frozen and stored at -80°C. Organoids were sectioned with a cryostat (Leica Biosystems #CM3050) at 18 µM onto glass slides. Organoids sections were washed three times for ten minutes in 1X PBS prior to a two-hour incubation in 10% BSA in PBS blocking solution (ThermoFisher Scientific BP1605-100). The sections were then incubated in primary antibodies diluted in blocking solution overnight at 4°C. The next day, sections were washed three times with 1X PBS for thirty minutes. They were then incubated in a solution of secondary antibodies diluted in a blocking solution at room temperature for two hours. The sections were

washed an additional three times in 1X PBS for thirty minutes.

Primary antibodies used were: rabbit anti SOX2 (ab97959, 1:250 dilution), chicken anti Nestin (ab134017, 1:250 dilution), and DAPI (Sigma D9542-10mg). Secondary antibodies used were: goat anti-rabbit Alexa Fluor 594 (ab150080, 1:250 dilution) and goat anti-chicken Alexa Fluor 488 (ab150169, 1:250 dilution). Imaging was done using the Zeiss Axioimager Z2 Widefield Microscope at the UC Santa Cruz Institute for the Biology of Stem Cells (RRID:SCR021135) and the Zen Pro software. Images were processed using ImageJ.

Chapter 3

Advanced Glycation End Products

Background

Recent studies have shown that concentrations of advanced glycation end products (AGE's) play a role in metabolic disorders such as diabetes and chronic kidney disease[41]. For example, affected individuals have been observed to contain micrograms per milliliter AGE levels, six orders of magnitude higher than healthy individuals as well as evidence that AGE's are able to modulate insulin production[42]. AGE's have also been shown to be sufficient to cause stress and toxicity in cell culture[43]. Here we demonstrate that AGE's are transiently made at low levels in cell culture conditions, that the production of AGE's scales exponentially with time between feeds and that small changes in sugar

concentration have a small effect on AGE production.

Results

At the conclusion of Autoculture experiments the concentration of AGE's were measured as a function of glucose concentration and feed frequency (figure 21a). AGE levels were found to vary from around 100 ng/mL at a 1 hour feed frequency to 10,000 ng/mL at 4 days. To generate a baseline measurement of the non-enzymatic production of AGE's, cell culture media containing FBS and varying glucose concentrations was incubated at 37C for 7 days without any cells. The concentration of glucose during these incubations did not significantly alter the production rate of AGE's.

A AGE levels in different conditions

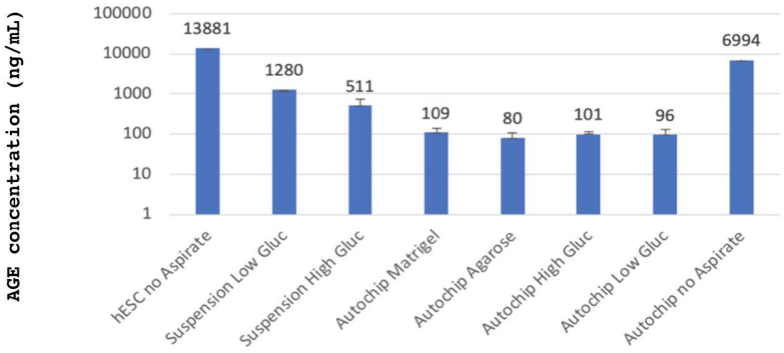

B [AGE] as a function of [glucose]

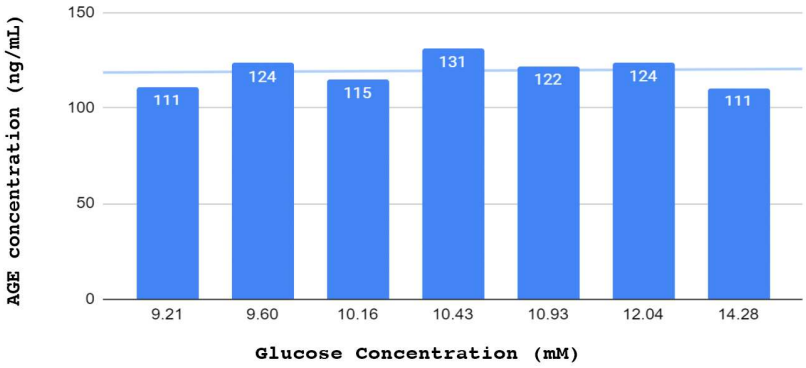

Figure 19: Advanced Glycation End Product levels in cell culture. *(A) Measured levels of AGE's as a function of culture condition including time since last feed, glucose level, and hydrogel. (B) Measured levels of AGE's as a function of glucose concentration in via cell free method of AGE production.*

Conclusions

Here we demonstrated with a limited set of data, that AGE production scales exponentially with time between feeds, and that little changes to sugar concentration have little to no effect on AGE production. This suggests that the production of AGE's is dependent on something being generated by the culture at an exponential rate, i.e. the cells or cell byproducts. While the measured concentrations of AGE's at 2 days was within a healthy range, the measured concentration at 4 days was within the pathological level reported in literature. This fits with anecdotal evidence that leaving a culture unfed for 4 days causes irreparable damage to the culture. The equation below represents a proposed biochemical equation for the explanation of non-enzymatic AGE production in cell culture where R is the rate of production:

$$R \cdot [Sugar] \cdot [Protein] \rightarrow [Advanced\ Glycation\ End\ Products]$$

Further studies would need to be performed to elucidate a value for R and to measure the effect of conditions such as temperature and time. An understanding of AGE's effect on cell culture could lead to greater understanding of how they affect human health.

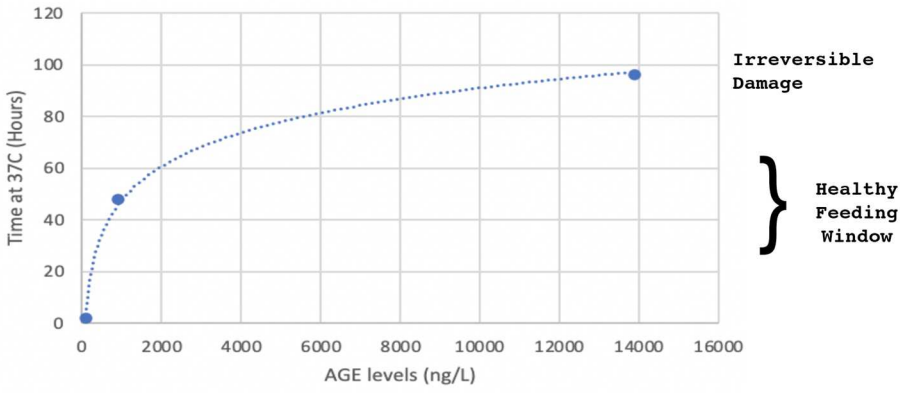

Figure 20: Model of AGE production over time in standard cell culture conditions. *Inferred levels of AGE's based on measurements in confluent 2D hESC cultures as measured by ELISA. A large spike observed between 48 and 96 hours agrees with previous observations*

Methods

Culturing experiments prepared and performed as described in chapter 3. Production of AGE's performed by incubating BSA at varying concentrations in DMEM at 37C for varying times. AGE concentrations measured by ELISA (Cloud-Clone Corp. part number CEB353Ge).

References

1. Suzuki IK et. al. Human-Specific NOTCH2NL Genes Expand Cortical Neurogenesis through Delta/Notch Regulation. Cell. 2018 May 31;173(6):1370-1384.e16. doi: 10.1016/j.cell.2018.03.067. Epub 2018 May 31. PMID: 29856955; PMCID: PMC6092419.
2. Seiler ST et. al. Modular automated microfluidic cell culture platform reduces glycolytic stress in cerebral cortex organoids bioRxiv 2022.07.13.499938; 10.1101/2022.07.13.499938
3. Fiddes IT et. al. Human-Specific NOTCH2NL Genes Affect Notch Signaling and Cortical Neurogenesis. Cell. 2018 May 31;173(6):1356-1369.e22. doi: 10.1016/j.cell.2018.03.051. Epub 2018 May 31. PMID: 29856954; PMCID: PMC5986104.
4. Artavanis-Tsakonas, Spyros et al. "Notch signaling: cell fate control and signal

integration in development.” Science 284 5415 (1999): 770–6.

5. Pollen, A. A. et al. Establishing cerebral organoids as models of human-specific brain evolution. Cell 176, 743–756 (2019).
6. Bhaduri, A. et al. Cell stress in cortical organoids impairs molecular subtype specification. Nature 578, 142–148 (2020).
7. Haldeman-Englert CR, Jewett T. 1q21.1 Recurrent Microdeletion. 2011 Feb 24 [Updated 2015 Nov 12]. In: Adam MP, Everman DB, Mirzaa GM, et al., editors. GeneReviews® [Internet]. Seattle (WA): University of Washington, Seattle; 1993–2022.
8. Funato, K. et. al. Human ESC-Based Model of H3.3G34R-Mutant High-Grade Glioma Reveals the Oncogenic Role Of Human-Specific NOTCH2NL Genes. Available at SSRN: https://ssrn.com/abstract=3654620
9. Stiles J, Jernigan TL. The basics of brain development. Neuropsychol Rev. 2010 Dec;20(4):327–48. doi: 10.1007/s11065-010-

9148-4. Epub 2010 Nov 3. PMID: 21042938; PMCID: PMC2989000.

10. Pollen AA, et. al. Molecular identity of human outer radial glia during cortical development. Cell. 2015 Sep 24;163(1):55-67. doi: 10.1016/j.cell.2015.09.004. PMID: 26406371; PMCID: PMC4583716.

11. Herculano-Houzel S. The human brain in numbers: a linearly scaled-up primate brain. Front Hum Neurosci. 2009 Nov 9;3:31. doi: 10.3389/neuro.09.031.2009. PMID: 19915731; PMCID: PMC2776484.

12. Mora-Bermúdez F, et. al. Differences and similarities between human and chimpanzee neural progenitors during cerebral cortex development. Elife. 2016 Sep 26;5:e18683. doi: 10.7554/eLife.18683. PMID: 27669147; PMCID: PMC5110243.

13. Gey, G. O., Coffman, W. D. & Kubicek, M. T. Tissue culture studies of the proliferative capacity of cervical carcinoma and normal epithelium. Cancer Res. 12, 264-265 (1952).

14. Scherer, W. F., Syverton, J. T. & Gey, G. O. Studies on the propagation in vitro of poliomyelitis viruses. iv. viral multiplication in a stable strain of human malignant epithelial cells (strain hela) derived from an epidermoid carcinoma of the cervix. Exp. Medicine 97, 695–710 (1953).

15. Ringe, J., Kaps, C., Burmester, G.–R. & Sittinger, M. Stem cells for regenerative medicine: advances in the engineering of tissues and organs. Naturwissenschaften 89, 338–351 (2002).

16. Patel, M. & Yang, S. Advances in reprogramming somatic cells to induced pluripotent stem cells. Stem Cell Rev. Reports 6, 367–380 (2010)

17. Rossi, G., Manfrin, A. & Lutolf, M. P. Progress and potential in organoid research. Nat. Rev. Genet. 19, 671–687 (2018).

18. Hofer, M. & Lutolf, M. P. Engineering organoids. Nat. Rev. Mater. 6, 402–420 (2021).

19. Lancaster, M. A. & Huch, M. Disease modelling in human organoids. Dis. models & mechanisms 12, dmm039347 (2019).

20. Qian, X., Song, H. & Ming, G.-l. Brain organoids: advances, applications and challenges. Development 146, dev166074 (2019).

21. Marton, R. M. & Pas, ca, S. P. Organoid and assembloid technologies for investigating cellular crosstalk in human brain development and disease. Trends Cell Biol. 30, 133–143 (2020).

22. Renner, M. et al. Self-organized developmental patterning and differentiation in cerebral organoids. The EMBO journal 36, 1316–1329 (2017).

23. Kanton, S. et al. Organoid single-cell genomic atlas uncovers human-specific features of brain development. Nature 574, 418–422 (2019).

24. Nascimento, J. M. et al. Human cerebral organoids and fetal brain tissue share

proteomic similarities. Front. cell developmental biology 303 (2019).

25. Kadoshima, T. et al. Self-organization of axial polarity, inside-out layer pattern, and species-specific progenitor dynamics in human es cell-derived neocortex. Proc. Natl. Acad. Sci. 110, 20284-20289 (2013).

26. Lancaster, M. A. et al. Cerebral organoids model human brain development and microcephaly. Nature 501, 373-379 (2013).

27. Neal, J. T. et al. Organoid modeling of the tumor immune microenvironment. Cell 175, 1972-1988 (2018).

28. Giandomenico, S. L., Sutcliffe, M. & Lancaster, M. A. Generation and long-term culture of advanced cerebral organoids for studying later stages of neural development. Nat. protocols 16, 579-602 (2021).

29. Field, A. R. et al. Structurally conserved primate lncrnas are transiently expressed during human cortical differentiation and

influence cell-type-specific genes. Stem cell reports 12, 245–257 (2019).

30. Uzquiano, A. et al. Single-cell multiomics atlas of organoid development uncovers longitudinal molecular programs of cellular diversification of the human cerebral cortex. bioRxiv (2022).

31. Ly, V. T. et al. Picroscope: low-cost system for simultaneous longitudinal biological imaging. Commun. biology 4, 1–11 (2021).

32. Baudin, P. V. et al. Low cost cloud based remote microscopy for biological sciences. Internet Things 18, 100454 (2022).

33. Chen, T. et al. Cell stress in cortical organoids impairs molecular subtype specification. (2020).

34. Picelli, S. et al. Full-length rna-seq from single cells using smart-seq2. Nat. Protoc. 9, 171–181 (2014).

35. Li, H. et al. The sequence alignment/map format and samtools. Bioinformatics 25, 2078–2079 (2009).

36. Dobin, A. et al. Star: ultrafast universal rna-seq aligner. Bioinformatics 29, 15–21 (2013).

37. Vivian, J. et al. Toil enables reproducible, open source, big biomedical data analyses. Nat. biotechnology 35, 314–316 (2017).

38. Dobin, A., Hitz, B. & Dewey, C. Star based encode long rna-seq processing pipeline (2016).

39. Stewart, L. J. et al. Role of glutathione in buffering excess intracellular copper in streptococcus pyogenes. MBio 11, e02804–20 (2020).

40. Reimand, J., Kull, M., Peterson, H., Hansen, J. & Vilo, J. g: Profiler—a web-based toolset for functional profiling of gene lists from large-scale experiments. Nucleic acids research 35, W193–W200 (2007).

41. Noordzij, M. J., J. D. Lefrandt, and A. J. Smit. "Advanced glycation end products in renal failure: an overview." Journal of renal care 34.4 (2008): 207–212.

42. Puddu, A., et al. "Advanced glycation end-products affect transcription factors regulating insulin gene expression." Biochemical and biophysical research communications 395.1 (2010): 122-125.

43. Yamagishi, Sho-ichi, et al. "Advanced glycation end products-induced apoptosis and overexpression of vascular endothelial growth factor in bovine retinal pericytes." Biochemical and biophysical research communications 290.3 (2002): 973-978.